Journal of Metals, Materials and Minerals, 35(1), e2216, 2025

Supporting Information

Hydroxyl combined with nitrogen on biomass carbon promotes the electrocatalytic H_2O_2 selectivity

Jiabi JIANG[1], Danni DENG[1], Yuchao WANG[1], Yingbi CHEN[1], Yu BAI[1], Meng WANG[1], Xiang XIONG[1], and Yongpeng LEI[1,*]

[1] *State Key Laboratory of Powder Metallurgy, Central South University, Changsha, Hunan, 410083, China*

***Corresponding author e-mail**: leiyongpeng@csu.edu.cn

Experimental

Material characterizations: Scanning electron microscopy (SEM) and energy-dispersive X-ray spectroscopy (EDS) element mapping was performed on COXEM EM-30; The American Micromeritics ASAP 2460 was used to measure BrunauerEmmett-Teller (BET) specific surface area and pore size distribution. The FTIR was performed in the American Thermo Fisher Scientific Nicolet iS20; X-ray photoelectron spectroscopy (XPS) was collected on an Axia Ultra (Thermo Scientific ESCALab 250Xi+) XPS spectrometer equipped with an Al Kα source (1486.6 eV); The Zeta potential was carried out on a Malvern Zetasizer Nano ZS90 Zeta potential analyzer.

Electrochemical measurements: The ORR performances were evaluated with a three-electrode cell equipped with a rotating ring-disk electrode (RRDE) (Pine Research Instrumentation, USA) and CHI730E electrochemical workstation (Chenhua, Shanghai). Carbon rod was used as counter electrode, a saturated calomel electrode (SCE) was used as reference electrode, and the working electrode was RRDE loaded with catalyst. For preparing the working electrode, the catalyst ink was prepared by dispersing 6.0 mg of catalyst into 960 μL water-isopropanol solution (volume ratio of 3:1) and 40 μL Nafion (5 wt%) solution and sonicating for 30 min. After polishing RRDE mechanically with alumina suspension, 10 μL of catalyst ink was drop-casted onto the disk electrode (0.247 cm^2 area) of RRDE, resulting a catalyst loading of 24.2 $\mu g \cdot cm^{-2}$ and then the electrode was dried under an infrared lamp to give a uniform catalyst layer. Prior to the ORR measurement, the 0.1 M KOH electrolyte was saturated with O_2 for 30 min and kept saturated with O_2 during all the testing processes. Cyclic voltammetry (CV) scans at a rate of 100 $mV \cdot s^{-1}$ from 1.2 V to 0 V vs. RHE were performed until a stable state was reached. Then, the LSV polarization curves were scanned from 1.0 V to 0 V vs. RHE at a rate of 5 $mV \cdot s^{-1}$ with the RRDE rotating at 1600 rpm. The Pt ring electrode was held at 1.3 V vs. RHE to quantify the amounts of H_2O_2 produced on the disk electrode. The collection efficiency (N) on the RRDE electrode was calibrated in 0.1 M KCl + 10 mM $K_3Fe(CN)_6$ electrolyte at different rotation rates. Thus, the measured collection efficiency was determined to be 36%, which is reasonably close to the theoretical value. The H_2O_2 selectivity was calculated using the following Equation :

$$H_2O_2(\%) = 200 \times \frac{\frac{I_r}{N}}{I_d + \frac{I_r}{N}} \quad (1)$$

Where I_r is the ring current, I_d is the disk current and N is the collection efficiency. The number of electrons transferred (n) was calculated using the Equation:

$$n = 4 \times \frac{I_d}{I_d + \frac{I_r}{N}} \quad (2)$$

Electrochemical active surface area (ECSA) was conducted from double-layer charging curves using the CVs at the non-Faradic potential window in 0.1 M KOH. These samples were tested with scan rates ranging from 10 to 100 $mV \cdot s^{-1}$. The plots of current density (at 1.05 V) as a function of the scan rate showed the double-layer capacitance (C_{dl}) by the slopes.

All recorded potentials were calibrated to the reversible hydrogen electrode (RHE) using the Equation $E_{RHE} = E_{SCE} + 0.0591*pH$.

Electrochemical measurements in Flow Cell: The electroreduction was further carried out in a gas diffusion electrode consisting of a coated HNC catalyst as the working electrode, an anion exchange membrane, and commercial Nickel foams as the anode. Working electrode was prepared by spraying the catalyst onto a gas diffusion layer. Catalyst ink was prepared by mixing 10 mg catalyst, 100 μL 5 wt% Nafion solution and 2 mL ethanol. The ink is ultrasonically treated for 30 min before spraying, then sprayed on a gas diffusion (2 $cm^2 \times 3$ cm^2). The working electrode, an anion exchange membrane, and an anode of Nickel foams were then held together with a Polytetrafluoroethylene gasket. The liquid electrolyte can be introduced into a chamber between the anode and the membrane and between the membrane and the cathode. The air diffuses from behind the gas diffusion layer to the liquid electrolyte in the catalytic region (1 $cm^2 \times 2$ cm^2). All the electrochemical experiments were tested at the CHI730 electrochemical workstation (Chenhua, Shanghai). The electrolyte (1 M KOH, 50 mL

electrolytes for cathode and anode, respectively) was circulated in the electrochemical cell using a peristaltic pump.

H_2O_2 concentration quantification: The cerium sulfate ($Ce(SO_4)_2$) was used as an indicator to measure H_2O_2 concentration quantitatively. The quantification method is based on the color change from a yellow Ce^{4+} solution to a colourless Ce^{3+} by adding H_2O_2 as the reductant: $2Ce^{4+} + H_2O_2 \rightarrow 2Ce^{3+} + 2H^+ + O_2$. The concentration of Ce^{4+} before and after the reaction can be measured by ultraviolet-visible spectroscopy. Standard $Ce(SO_4)_2$ solution (0.5 mM) was prepared by dissolving $Ce(SO_4)_2$ salts into 0.5 M H_2SO_4. The calibration curves between absorbance and Ce^{4+} concentration were determined by measuring the absorbance at 318 nm of different $Ce(SO_4)_2$ solutions with known concentrations (0.01 mM to 0.05 mM) by uv-vis (Shimadzu UV-1800). After electrolysis for a certain time period, 20 µL of the electrolyte in the cathode chamber after neutralization by 0.5 M sulfuric acid solution was added into the standard $Ce(SO_4)_2$ titrant solution. Based on the linear relationship between the signal intensity and Ce^{4+} concentration, the molar amounts of consumed Ce^{4+} after reaction could be obtained. By this approach, the amounts of H_2O_2 produced can be calculated as half the molar amounts of the Ce^{4+} consumed ($2*C_{react(H2O2)} = C_{react(Ce4+)}$).

The degradation of TC/RhB/MB: The working electrode (1 $cm^2 \times$ 2 cm^2) was immersed in the cathode chamber which KOH (1 $mol \cdot L^{-1}$) and TC/RhB /MB (20 $mg \cdot L^{-1}$). The working electrode is maintained at a constant potential of 0.1V vs. RHE and continuously irradiated on the cathode side with a UV lamp (365 nm, 5 W). The change in the concentration of TC/RhB/MB was monitored by UV-vis spectrophotometry.

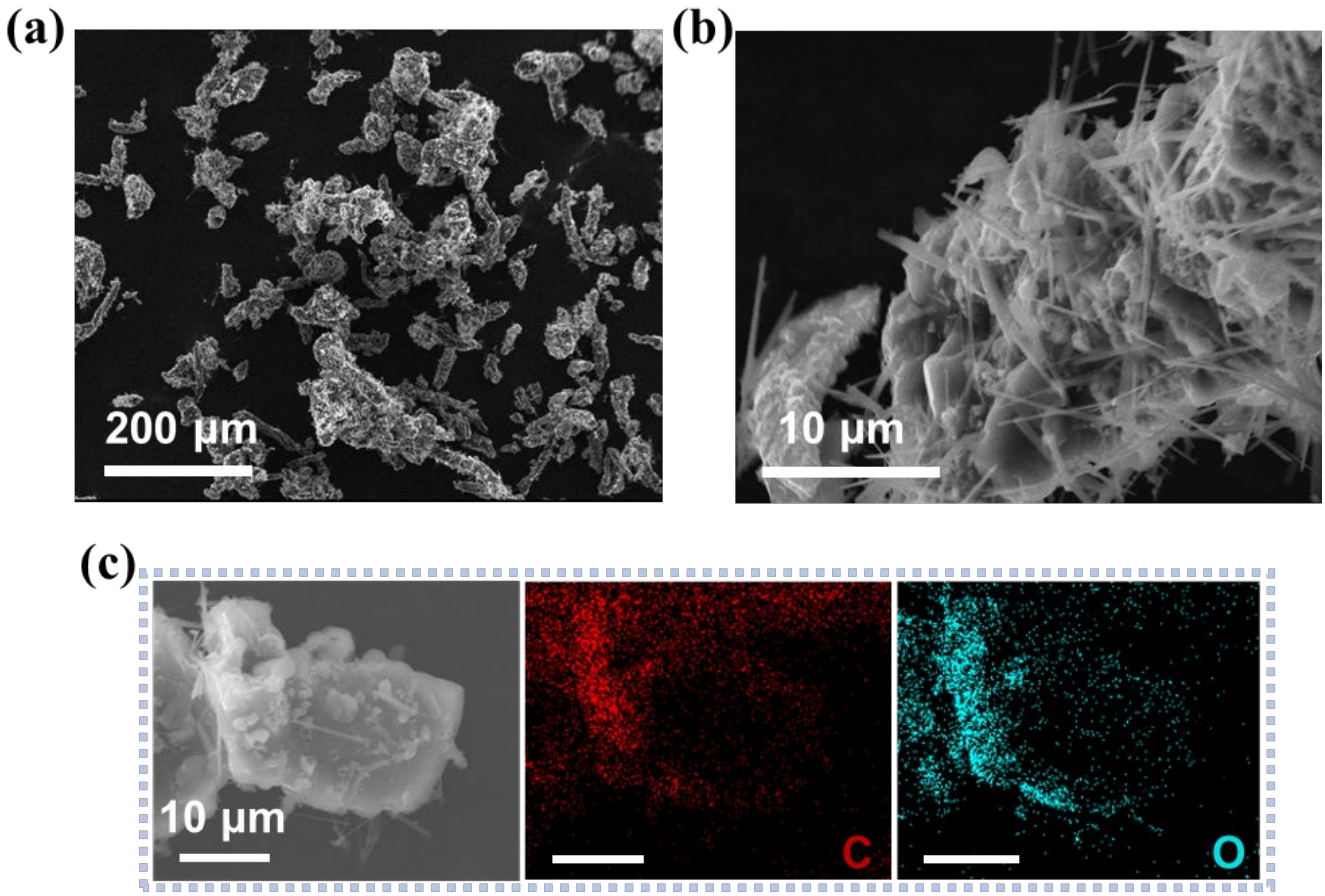

Figure S1. (a) and (b) SEM images, (c) EDS elemental mappings of HC.

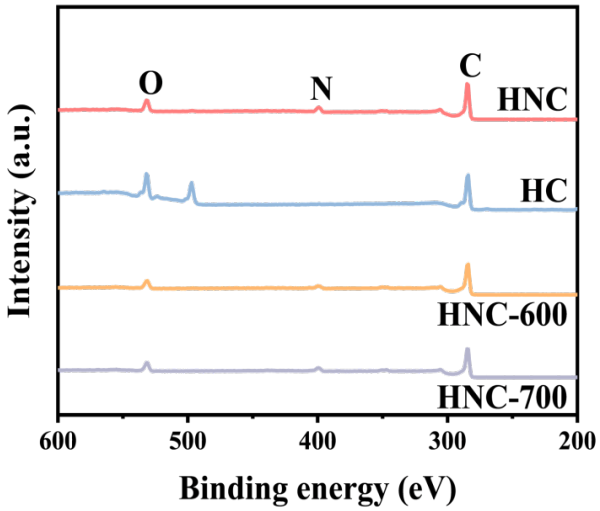

Figure S2. Survey XPS spectra.

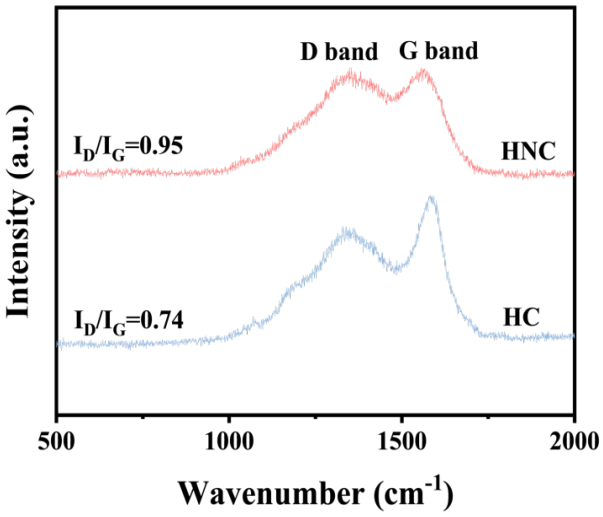

Figure S3. Raman spectra of HNC and HC.

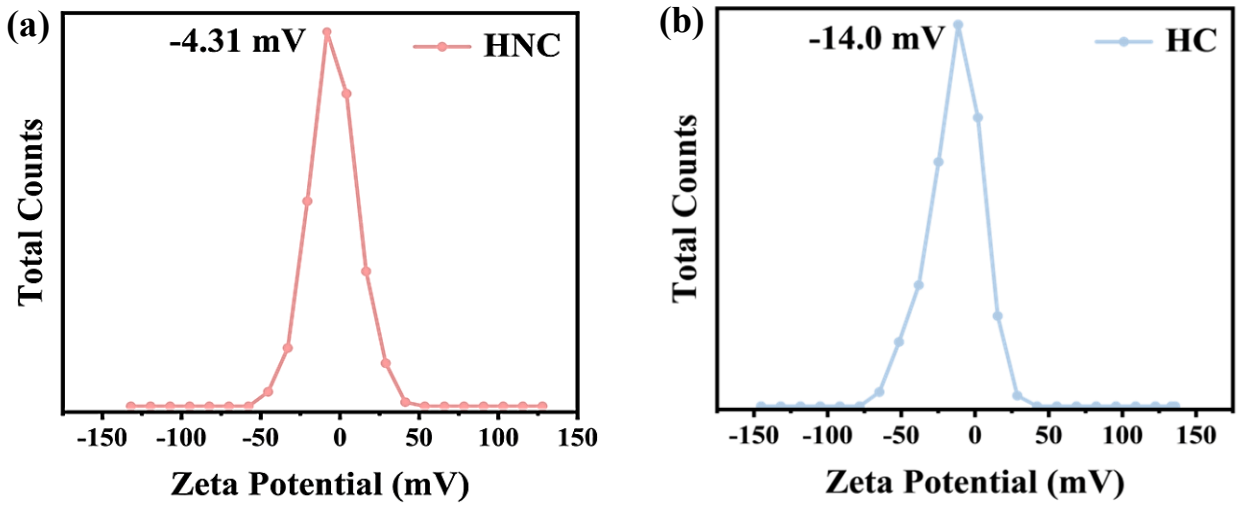

Figure S4. Zeta potential of (a) HNC and (b) HC.

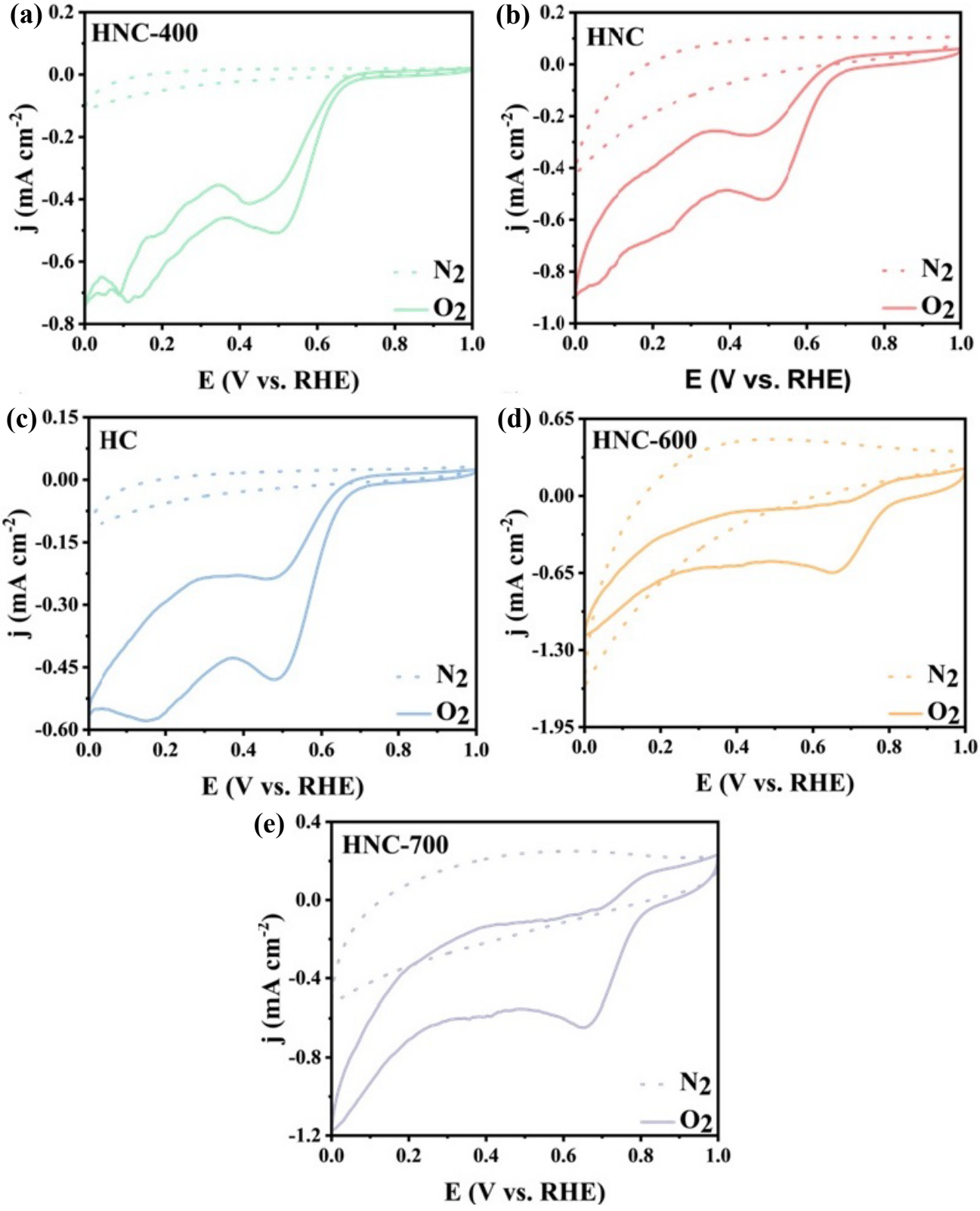

Figure S5. Cyclic voltammograms of (a) HNC-400, (b) HNC, (c) HC, (d) HNC-600 and (e) HNC-700 in O_2 and N_2 saturated 0.1 M KOH solution.

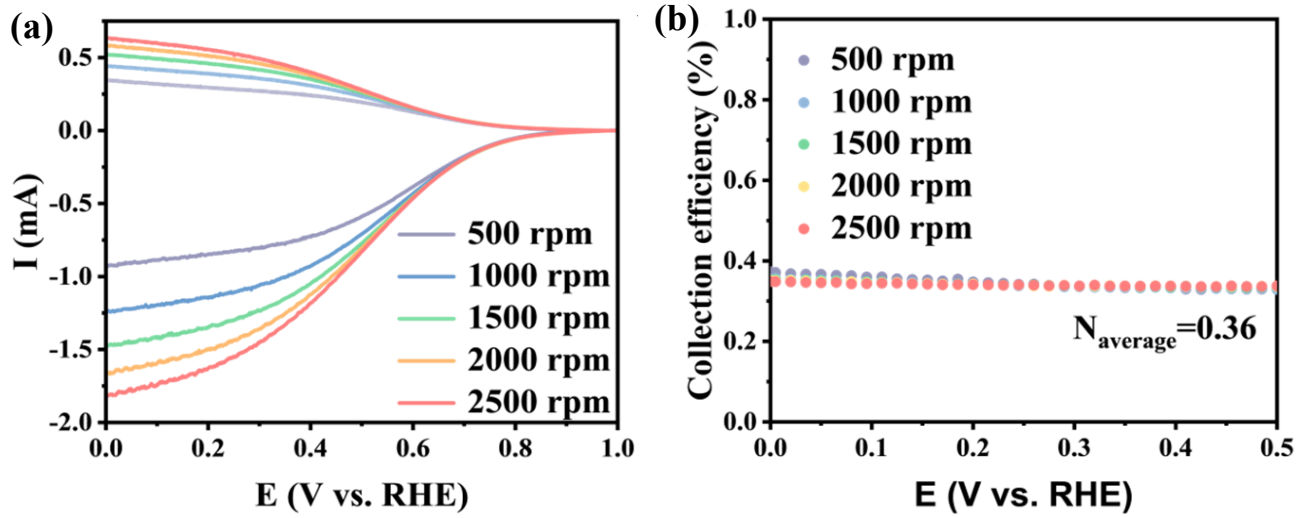

Figure S6. (a) RRDE voltammograms of glassy carbon electrode in 10 mM $K_3Fe(CN)_6$ and 0.1 M KCl with the disk and ring currents at 500, 1000, 1500, 2000 and 2500 rpm. The scan rate is 5 mV·s^{-1} (1.3 V vs. RHE for ring), (b) The corresponding collection efficiency of RRDE voltammograms as a function of the potential.

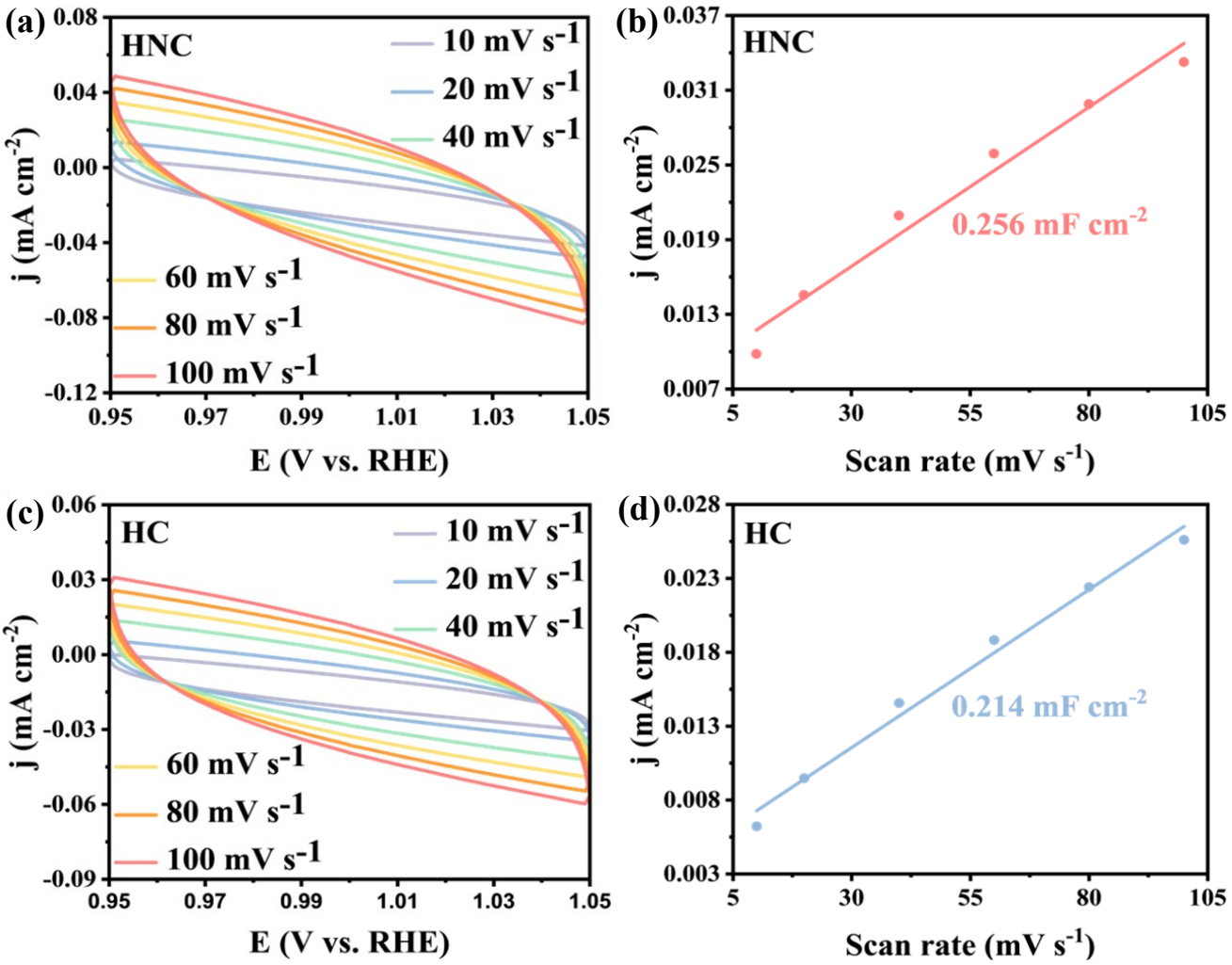

Figure S7. CV curves of (a) HNC and (c) HC in non-Faradaic potential region at different sweep rates ranging. Linear fitting of capacitive currents of (b) HNC and (d) HC vs. scan rate.

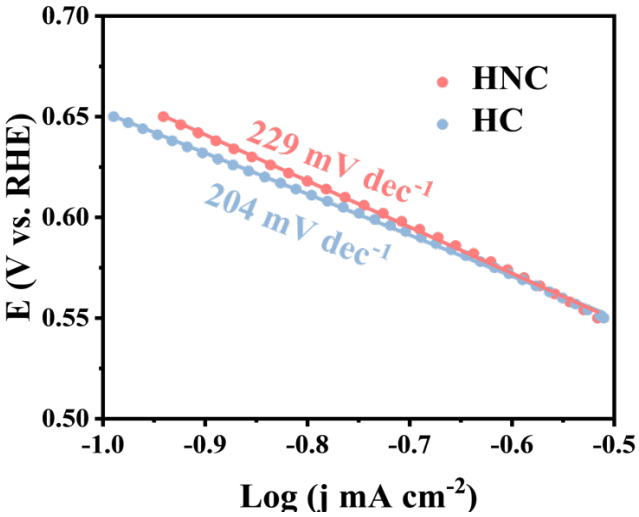

Figure S8. Tafel slopes of HNC and HC.

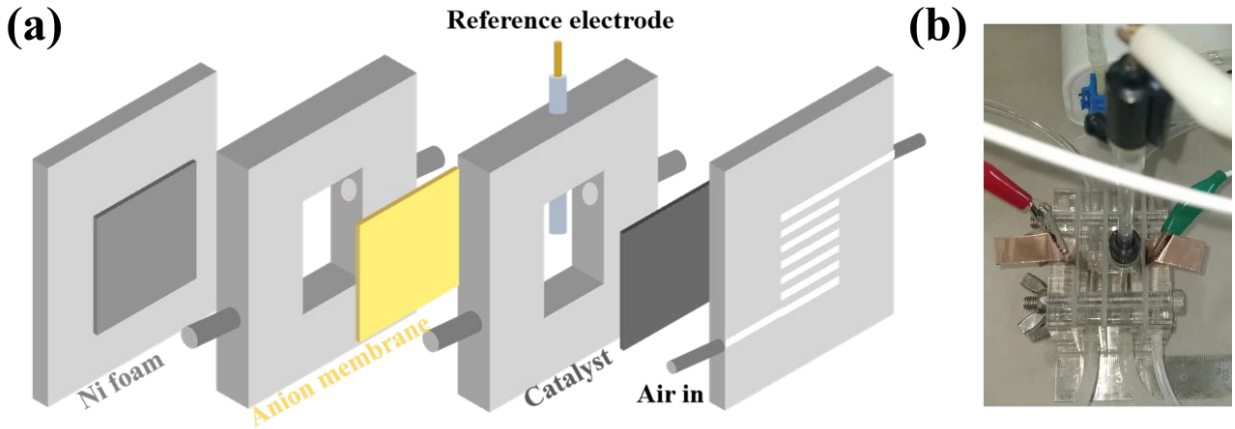

Figure S9. (a) The schematic diagram and (b) optical photograph of the flow cell.

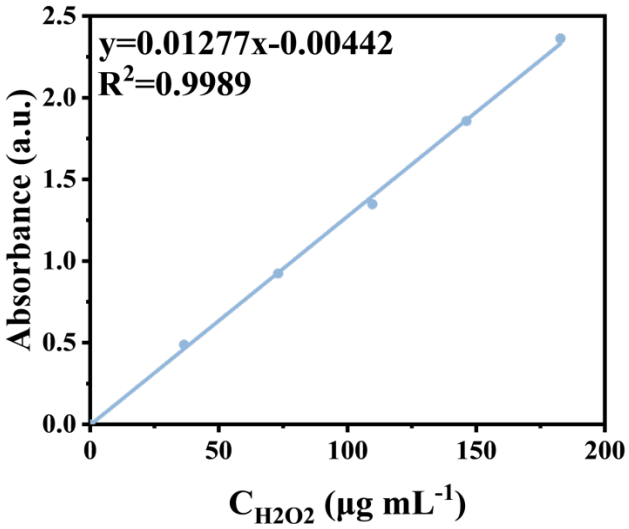

Figure S10. The concentration-absorbance calibration curve of $Ce(SO_4)_2$ with the given concentrations (0, 0.01, 0.02, 0.03, 0.04, and 0.05 mM).

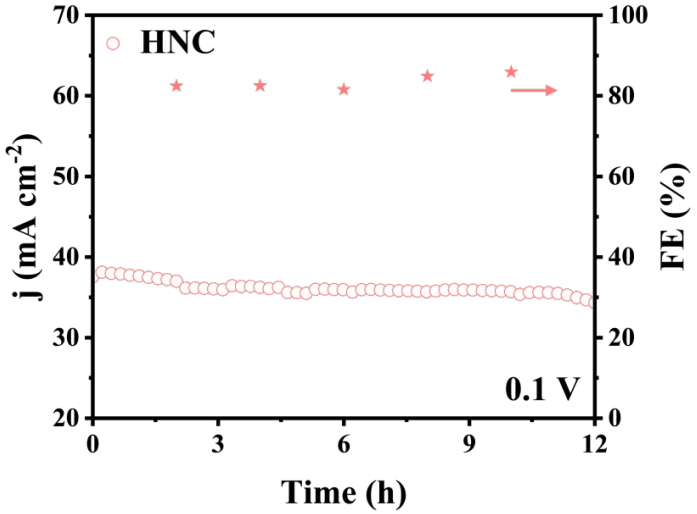

Figure S11. The variations in current density and Faradaic efficiency against time of HNC during the long-term potentiostatic test with the potential kept constant.

Table S1. Elemental composition from XPS.

Samples	**C** [at%]	**O** [at%]	**N** [at%]
HNC	79.3	11.4	9.3
HC	76.2	23.8	-
HNC-600	79.8	11.3	8.9
HNC-700	83.1	10.2	6.7

Table S2. Comparison of H_2O_2 selectivity and potential range from 2022 to 2024.

Catalysts	**Selectivity** [%]	**Potential (V vs. RHE)**	**Ref.**
HNC	**>92%**	**0 to 0.5**	**This Work**
$MHCS_{0.5}$	>95	0.3 to 0.8	Nature Communications, 2024, 15, 983.
GDY-50	>95.5	0.45 to 0.75	Angewandte Chemie International Edition, 2024, 63, e202401501.
P-NMG-10	80 to 91	0 to 0.7	Nature Communications, 2023, 14, 4430.
N/O-C	~80	0.3 to 0.6	Nano Letters, 2023, 23, 1100.
NBO-G/CNTs	85 to 93	0.35 to 0.75	Advanced Materials, 2023, 35, 2209086.
COPN-3	~90 to ~93	0 to 0.6	ACS Catalysis, 2023, 13, 14492.
CNB-ZIL	70 to 85	0 to 0.7	Angewandte Chemie International Edition, 2022, 61, e202206915.
CQDs	>90%	0.2 to 0.65	Energy & Environmental Science, 2022, 15, 4167.

Table S3. Comparison of H_2O_2 production in flow cell from 2022 to 2024.

Catalysts	**Yield rate** [$mol \cdot g^{-1} \cdot h^{-1}$]	**Stability**	**FE** (%)	**Ref.**
HNC	**0.797**	**12h@0.1V**	**~80**	**This Work**
Ni-TCPP(Co)	18.2	12h@0.1V	90	Angewandte Chemie International Edition, 2024, 63, e202408500.
Co-N_4-PC	11.2	12h@0.3V	75	Applied Catalysis B, 2023, 324, 122267.
COPN-3	17.7	-	73	ACS Catalysis, 2023, 13, 14492.
Sb-NSCF	7.46	75h@0.55V	>80	Nature Communications, 2023, 14, 368.
P-NMG-10	23	-	~85	Nature Communications, 2023, 14, 4430.
NBO-G/CNTs	0.709	30h@~200 $mA \cdot cm^{-2}$	81	Advanced Materials, 2023, 35, 2209086.
N,O-CNTs	0.265	24h@~48 $mA \cdot cm^{-2}$	95	Advanced Science, 2022, 9, 2201421.